Journal of *Marine Science and Engineering*

MDPI

Article

Representative Transmission Coefficient for Evaluating the Wave Attenuation Performance of 3D Floating Breakwaters in Regular and Irregular Waves

Huu Phu Nguyen [1,*], Jeong Cheol Park [1], Mengmeng Han [1], Chien Ming Wang [1], Nagi Abdussamie [2], Irene Penesis [2] and Damon Howe [2]

[1] School of Civil Engineering, The University of Queensland, St Lucia, QLD 4072, Australia; jeongcheol.park@uq.edu.au (J.C.P.); mengmeng.han@uq.edu.au (M.H.); cm.wang@uq.edu.au (C.M.W.)
[2] National Centre for Maritime Engineering and Hydrodynamics, Australian Maritime College, University of Tasmania, Locked Bag 1395, Launceston, TAS 7250, Australia; nagi.abdussamie@utas.edu.au (N.A.); I.Penesis@utas.edu.au (I.P.); damon.howe@utas.edu.au (D.H.)
* Correspondence: huuphu.nguyen@uq.net.au

Abstract: Wave attenuation performance is the prime consideration when designing any floating breakwater. For a 2D hydrodynamic analysis of a floating breakwater, the wave attenuation performance is evaluated by the transmission coefficient, which is defined as the ratio between the transmitted wave height and the incident wave height. For a 3D breakwater, some researchers still adopted this evaluation approach with the transmitted wave height taken at a surface point, while others used the mean transmission coefficient within a surface area. This paper aims to first examine the rationality of these two evaluation approaches via verified numerical simulations of 3D heave-only floating breakwaters in regular and irregular waves. A new index—*a representative transmission coefficient*—is then presented for one to easily compare the wave attenuation performances of different 3D floating breakwater designs.

Keywords: floating breakwater; wave attenuation performance; transmission coefficient; regular wave; irregular wave

Citation: Nguyen, H.P.; Park, J.C.; Han, M.; Wang, C.M.; Abdussamie, N.; Penesis, I.; Howe, D. Representative Transmission Coefficient for Evaluating the Wave Attenuation Performance of 3D Floating Breakwaters in Regular and Irregular Waves. *J. Mar. Sci. Eng.* **2021**, *9*, 388. https://doi.org/10.3390/jmse9040388

Academic Editors: Riccardo Briganti and Theophanis V. Karambas

Received: 16 February 2021
Accepted: 31 March 2021
Published: 6 April 2021

1. Introduction

Floating breakwaters have been used to provide safe harborage and to protect shorelines. When compared to the conventional bottom-founded breakwaters, floating breakwaters possess several advantages [1]: (i) being less costly when constructed at sites with soft seabed conditions and large water depth; (ii) the negligible effect of tidal variation and sea-level rise on these floating structures; (iii) little visual impact on the horizon from the shore as freeboards are rather small; (iv) being more environmentally friendly because of better water circulation and smaller benthic footprints; and (v) being easily expanded, rearranged, removed and relocated. However, floating breakwaters usually have a low wave attenuation performance for long waves (as compared to the breakwater width). In addition, their mooring systems may be more susceptible to damage under extreme wave action.

Most research studies on floating breakwaters are carried out in the 2D domain where the breakwater is assumed to be infinitely long. For 2D floating breakwaters under regular waves, the wave attenuation performance is evaluated by using the transmission coefficient (K_t) which is defined as the ratio between the transmitted wave height (H_t) and the incident wave height (H_I). Numerically or analytically, where the incident wave height is already given, the transmission coefficient can be obtained by determining the transmitted wave height at a surface point behind the breakwater (e.g., see [2]). Experimentally, the incident wave height and transmitted wave height can be determined from the measured wave elevations. These approaches for determining the transmission coefficients for

floating breakwaters are similar to those discussed for the traditional bottom-founded breakwaters [3–5].

As realistic floating breakwaters are 3D where the breakwater length is finite, several researchers have conducted experimental and numerical studies on 3D floating breakwaters [6–12]. In experimental studies, several researchers (e.g., [7,9]) used the transmission coefficient at a certain surface point for evaluating the wave attenuation performance of 3D floating breakwaters. In numerical studies, the mean transmission coefficient within a prescribed surface area has been adopted for the evaluation of the wave attenuation performance [10,13]. However, the rationality of these experimental and numerical evaluation approaches was not discussed.

This paper aims to numerically examine the aforementioned approaches as well as other possible approaches for quantitatively evaluating the wave attenuation performance of 3D floating breakwaters in regular and irregular waves. The examination is conducted by performing hydrodynamic analysis of heave-only floating box-type breakwaters, which are restrained by piles or mooring dolphins. The classical linear hydrodynamic theory is adopted for the analysis. In Section 2, we articulate the problem at hand, present the methodology for the solution and verify the results obtained. In Section 3, the transmitted wave fields behind 3D heave-only floating breakwaters are presented and various ways for quantifying the wave attenuation performance of a 3D floating breakwater are discussed. A new representative transmission coefficient is proposed for better evaluation of the wave attenuation performance of a 3D floating breakwater. Section 4 presents some concluding remarks.

2. Problem Definition, Methodology and Verification

Consider a box-type heave-only rigid floating breakwater and the global coordinate system $Oxyz$ as shown in Figure 1. The breakwater has length L, width B, draft d and is sited in a constant water depth h. The water domain is assumed to be infinite along x- and y-directions. The incident wave has a significant wave period T_s and significant wave height $H_{I,s}$. The incident wave angle with the x-axis is denoted by θ. The problem at hand is to determine the transmitted wave field and use this information to quantify the performance of the 3D floating breakwater under regular and irregular waves.

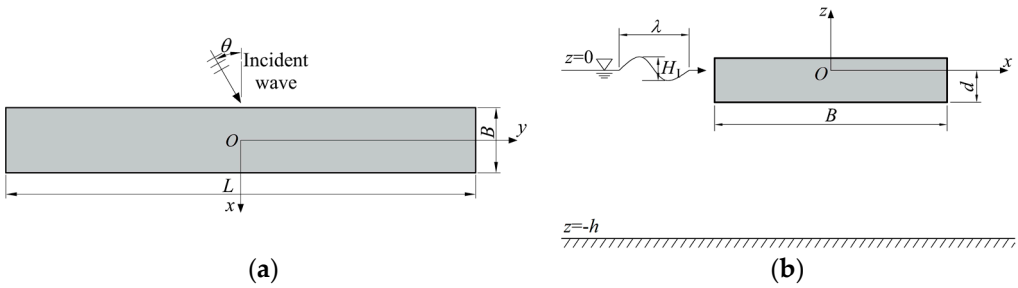

Figure 1. (**a**) Plan view, (**b**) side view of floating breakwater.

The breakwater is assumed to be deployed in locations where irregular waves can be represented by the Bretschneider spectrum [14]. Examples of such locations are the west coast of Ireland [15], and the Dutch coast [16]. The spectral density of the Bretschneider spectrum is given by:

$$S(\omega_i) = 0.1687 \frac{H_{I,s}^2 \omega_s^4}{\omega_i^5} \exp\left(-0.675 \frac{\omega_s^4}{\omega_i^4}\right), \; i = \{1, 2, ..., n_\omega\}, \tag{1}$$

where ω_i is the wave frequency of the ith spectral component, $\omega_s = 2\pi/T_s$, n_ω is the number of discrete spectral components for accurate representation of continuous wave spectrum. The resolution frequency is $\Delta\omega = (\omega^U - \omega^L)/n_\omega$, where ω^L and ω^U are respectively the

lower and upper bounds of wave frequencies where the spectral density value vanishes. The ith spectral component has the wave height $H_I(\omega_i) = 2\sqrt{2S(\omega_i)\Delta\omega}$.

Regular waves are also considered for a comparison study. The wave period, wave height, wavelength and frequency for a regular wave are denoted as T, H_I, λ and ω, respectively. In comparing the wave attenuation performances of the floating breakwater under irregular waves and regular waves, we shall use a representative regular wave where its wave period and height are, respectively, equal to the significant wave height $H_{I,s}$ and the significant wave period T_s [4,17–19].

To quantify the effectiveness of a floating breakwater in attenuating a regular wave at a given surface point, the following transmission coefficient K_t is used:

$$K_t = \frac{H_t}{H_I}, \tag{2}$$

where H_t is the transmitted wave height at the point considered.

For irregular waves, the transmission coefficient at a given surface point is defined as:

$$K_t = \frac{H_{t,s}}{H_{I,s}}, \tag{3}$$

where the significant transmitted wave height $H_{t,s}$ is given by:

$$H_{t,s} = 4\sqrt{\sum_{i=1}^{n_\omega} [H_t(\omega_i)/H_I(\omega_i)]^2 S(\omega_i)\Delta\omega}, \tag{4}$$

where $H_t(\omega_i)$ is the transmitted wave height at the considered point for the component wave frequency ω_i. The squared term under the square root in Equation (4) is usually referred to as a transfer function between the spectrum of the transmitted waves $S_t(\omega)$ and the incident wave spectrum $S(\omega)$. We have the following relation:

$$S_t(\omega) = [H_t(\omega)/H_I(\omega)]^2 S(\omega). \tag{5}$$

From Equations (3)–(5), we can see that the transmission coefficient is also equal to the square root of the ratio between the energy of the transmitted waves and that of the incident waves.

In the hydrodynamic analysis, the fluid is assumed to be inviscid and incompressible, and the fluid motion is irrotational. The classical linear potential wave theory is adopted for modelling the fluid motion. The breakwater is modelled as a plate [20]. Note that the linear wave theory has been widely adopted for estimating the transmission coefficients of floating breakwaters, e.g., in research study [1] and in design guidelines [21]. It is expected that the accuracy of transmission coefficients obtained by using the linear wave theory decreases as the wave steepness (i.e., the ratio between the wave height and wavelength) increases. However, the limit of wave steepness where the linear wave theory can still be valid has not been clearly established due to the lack of comparison between numerically estimated and measured transmission coefficients. The validity of the linear wave theory is also affected by the breakwater configuration and cross-sectional shape. An existing comparative study [22] between measured and numerically estimated transmission coefficients obtained by using the linear wave theory showed that for box-type floating breakwaters and wave steepness of about 0.04, a good agreement between experimental and numerical results was obtained. For a larger wave steepness of about 0.07 and the Berkeley Wedge breakwater, the difference between the numerically estimated and measured transmission coefficients was shown to be up to 35% at resonance [23].

The finite element-boundary element (FE-BE) method is adopted for solving the fluid–structure interaction problem in the frequency domain. As this method is well-known, only a brief of the method is presented in this paper for brevity. Details of the FE-BE method may be obtained from the literature, such as from papers by Kim et al. [24], and

Nguyen et al. [25]. Note that the FE-BE method has been developed for a general case where elastic deformations of floating structures and flexible connections between structure modules can be accounted for. When using this method for the present hydrodynamic problem (where the breakwater is assumed to be rigid), the rigidity of the structure is simply set to an infinitely large value.

According to the FE-BE method, the equation of motion for floating breakwaters in the frequency domain may be written in the following matrix form [25]:

$$\left[-\omega^2(\mathbf{M}+\mathbf{M}_\mathrm{a})-\mathrm{i}\omega\mathbf{C}_\mathrm{d}+\mathbf{K}+\mathbf{K}_\mathrm{rf}\right]\mathbf{u}=\mathbf{F}_\mathrm{exc}, \tag{6}$$

where i is the imaginary unit (i = $\sqrt{-1}$) $\mathbf{M}$ is the global mass matrix, $\mathbf{M}_\mathrm{a}$ is the matrix of added mass, $\mathbf{C}_\mathrm{d}$ is the matrix of hydrodynamic damping, $\mathbf{K}$ is the global stiffness matrix, $\mathbf{K}_\mathrm{rf}$ is the global matrix of the restoring force resulting from the combination of the buoyancy force and the gravitation force acting on the breakwater, $\mathbf{u}$ is the nodal vector of the complex amplitudes of the displacements, $\mathbf{F}_\mathrm{exc}$ is the vector of the complex amplitude of the excitation wave force. The vectors of breakwater displacements and excitation wave forces acting on the breakwater at the time t are, respectively, given by:

$$\mathbf{u}_\mathrm{re}=\mathrm{Re}\left(\mathbf{u}e^{-\mathrm{i}\omega t}\right), \tag{7}$$

$$\mathbf{F}_\mathrm{exc,re}=\mathrm{Re}\left(\mathbf{F}_\mathrm{exc}e^{-\mathrm{i}\omega t}\right), \tag{8}$$

where Re(.) indicates the real part.

The matrices $\mathbf{K}$, $\mathbf{K}_\mathrm{rf}$ and $\mathbf{M}$ are obtained using the finite element method [25]. The boundary condition due to the presence of the mooring system that the breakwater only moves up and down is imposed in the numerical model by modifying the stiffness matrix $\mathbf{K}$ using the penalty method [26]. The added mass and hydrodynamic damping matrices $\mathbf{M}_\mathrm{a}$ and $\mathbf{C}_\mathrm{d}$ are obtained by applying the boundary element method procedure for the linear hydrodynamic problem where the fluid motion can be expressed in terms of the velocity potential φ_re. In the frequency domain, the velocity potential can be written in the following form:

$$\phi_\mathrm{re}=\mathrm{Re}\left(\phi e^{-\mathrm{i}\omega t}\right) \tag{9}$$

where φ is the complex amplitude of the velocity potential and is usually referred to as the spatial velocity potential that must satisfy the Laplace equation and boundary conditions on the linearized free surface, the seabed, at infinity, and on the wetted surface of the breakwater, as follows [27,28]:

$$\nabla^2\phi(x,y,z)=0 \tag{10}$$

$$\frac{\partial\phi}{\partial z}=\frac{\omega^2}{g}\phi \text{ on the linearized free surface } (z=0), \tag{11}$$

$$\frac{\partial\phi}{\partial z}=0 \text{ on the seabed,} \tag{12}$$

$$\frac{\partial\phi}{\partial n}=-\mathrm{i}\omega u_j n_j \text{ on the wetted surface of the breakwater,} \tag{13}$$

$$\lim_{|\mathbf{x}|\to\infty}\sqrt{|\mathbf{x}|}\left[\frac{\partial(\phi-\phi_\mathrm{in})}{\partial|\mathbf{x}|}-\mathrm{i}k(\phi-\phi_\mathrm{in})\right]=0, \tag{14}$$

where g is the gravitational acceleration (g = 9.81 m/s^2), $\partial/\partial n$ indicates the differential along the unit formal vector pointing from the structure to the fluid, u_j (where j = {1, 2, 3}) are the complex amplitudes of the displacements along the x-, y- and z- directions, n_j indicates the unit normal vector, $|\mathbf{x}|$ is given by $|\mathbf{x}|=\sqrt{x^2+y^2}$, k is the wave number and can be

obtained by solving the dispersion relation $k\tanh(kH) = \omega^2/g$, φ_{in} is the complex amplitude of the incident velocity potential and is given by:

$$\phi_{in} = \frac{gA}{\omega}\frac{\cosh k(z+H)}{\cosh kH}e^{ik(x\cos\theta + y\sin\theta)}. \quad (15)$$

The complex amplitude p_d of the hydrodynamic water pressure can be calculated from the spatial velocity potential using the following equation [28]:

$$p_d = -i\omega\rho_w\phi. \quad (16)$$

where ρ_w (= 1025 kg/m^3) is the mass density of water.

The FE-BE method was implemented in MATLAB, and its convergence, accuracy and validity were confirmed by comparing with the results reported by Diamantoulaki et al. [6] who also used the boundary element method (BEM) for solving the fluid part, but a semi-analytical approach for solving the structure part. The breakwater has L = 20 m, B = 4 m, d = 0.77 m and is subjected to regular waves with $\theta = \{0°, 45°\}$, and B/λ = [0.1, 1.1]. The water depth h = 10 m. The transmission coefficients along y = 0 and 2 m $\leq x \leq$ 40 m are presented in Figure 2. The normalized heave motion amplitudes ($|u_3|/A$) of the breakwater are given in Figure 3. The results reported by Diamantoulaki et al. [6] are indicated by '3D Ref.', while the results from the present study are indicated by '3D Present'. It can be seen that the present results are in good agreement with the results obtained by Diamantoulaki et al. [6].

The accuracy and validity of the developed FE-BE method have also been confirmed by comparing with the published numerical and experimental results for several other structures such as floating pontoon-type structures, interconnected floating structures, and oscillating wave surge converters. Details of the verification for these problems have been presented by Nguyen and Wang [29,30].

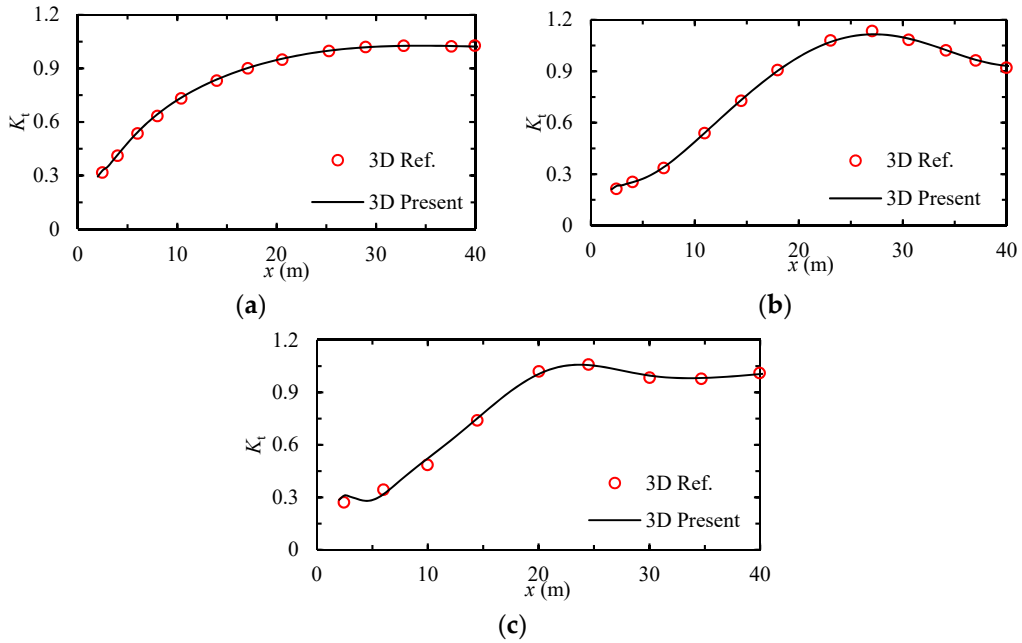

Figure 2. Transmission coefficients along y = 0 and 2 m $\leq x \leq$ 40 m, θ = 45°: (**a**) B/λ = 0.3, (**b**) B/λ = 0.6, (**c**) B/λ = 1.1.

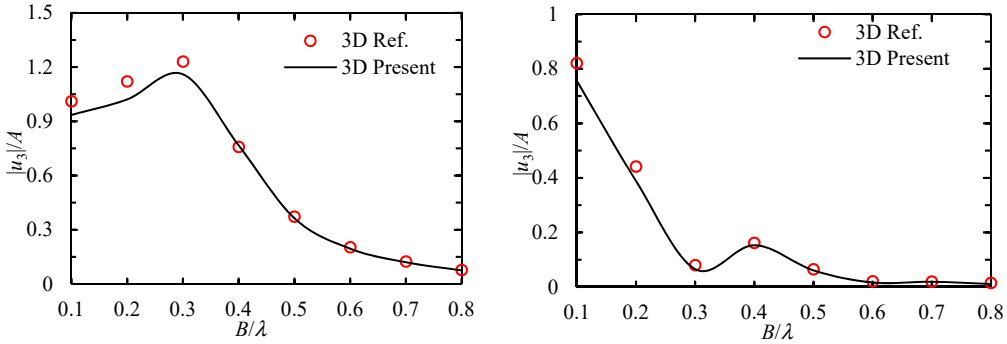

Figure 3. Normalized heave motion amplitudes of floating breakwater: (**a**) $\theta = 0°$, (**b**) $\theta = 45°$.

3. Results and Discussions

Numerical studies were carried out for three large heave-only floating breakwaters (FB#1, FB#2, FB#1L) with their dimensions as shown in Table 1. FB#1 has a width of 20 m and a draft of 10 m whilst FB#2 has a larger width of 30 m but a smaller draft of 6.7 m. Both the floating breakwaters have the same length of 200 m and about the same volume of displaced water. FB#1L has the same width and draft as FB#1 but it has a longer length of 500 m. The interaction between the freeboard and the water (e.g., overtopping) was not considered in the numerical model for simplicity and due to the limitation of the linear wave theory. Thus, the freeboard depth is not specified in Table 1. The water depth is assumed to be 40 m. The incident wave angles $\theta = \{0, 30\}$ ° are considered. A wide range of wave frequencies (ω = [0.31–1.48] rad/s) is examined. The significant wave height is taken as 1 m (i.e., $H_{I,s} = H_I = 1$ m).

Table 1. Design parameters (in meter) used for numerical studies.

Parameter	FB#1	FB#2	FB#1L
L	200	200	500
B	20	30	20
d	10	6.7	10

In the numerical model, the eight-node linear serendipity elements were adopted for discretization [25]. To select appropriate meshes of elements, convergence studies were performed. Figure 4 shows the transmission coefficients along $y = 0$ and 10 m $< x \leq$ 200 m for FB#1, $\theta = 0°$, $\omega = \{1.57, 1.05\}$ rad/s, and for four meshes of elements. Square elements were used sizes of 10 m, 5 m, 3.33 m and 2m for the four element meshes, respectively. For $\omega = 1.57$ rad/s, Figure 4a shows that the mesh of elements with a size smaller than 5 m is able to give converged results. For $\omega = 1.05$ rad/s, converged results can generally be obtained by using the mesh of elements with the largest size (10 m $\times$ 10 m). The observation in Figure 4 agrees well with the recommended size of elements (at least $\lambda/4$) given by Utsunomiya [31]. Based on the convergence study and the recommendation in the literature [31], the element size is taken to be smaller than $\lambda/4$ in the next sections. For irregular waves, 100 regular wave components were used for the accurate representation of the continuous wave spectrum. The upper and lower bounds of wave frequencies are 3.12 rad/s and 0.31 rad/s, respectively. These bounds were selected so that the wave spectrum density is almost zero at these frequencies. The computations were performed on the high-performance computing (HPC) system at The University of Queensland.

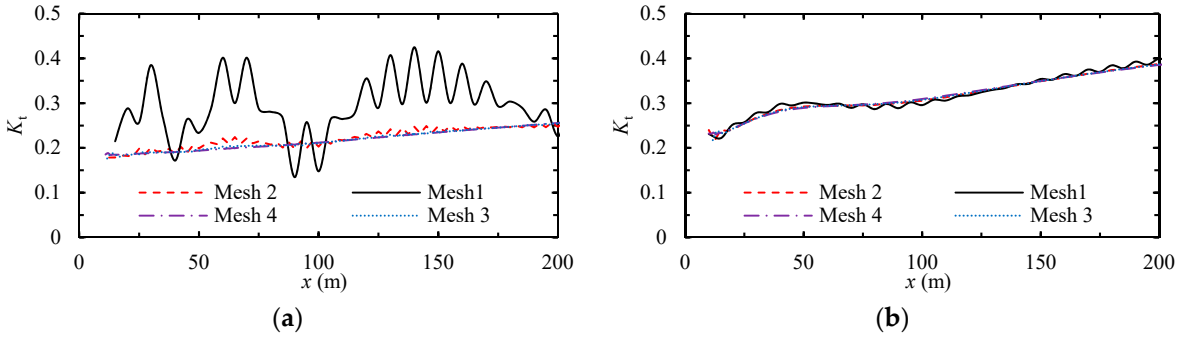

Figure 4. Transmission coefficients for mesh 1 (10 m × 10 m), mesh 2 (5 m × 5 m), mesh 3 (3.33 m × 3.33 m), mesh 4 (2 m × 2 m): (**a**) ω = 1.57 rad/s, (**b**) ω = 1.05 rad/s.

3.1. Transmitted Wave Field in Regular and Irregular Waves

Figures 5 and 6 show the contours of the wave elevation amplitude normalized with respect to the incident wave amplitude of regular waves for FB#1 and FB#1L. The contours of the normalized wave elevation amplitude behind the breakwaters reflect the transmission coefficients. It can be seen from Figure 5 that the transmission coefficients generally decrease as B/λ increases from 0.2 to 0.63. This result is expected, and has been widely seen for 2D floating breakwaters (e.g., see [32,33]).

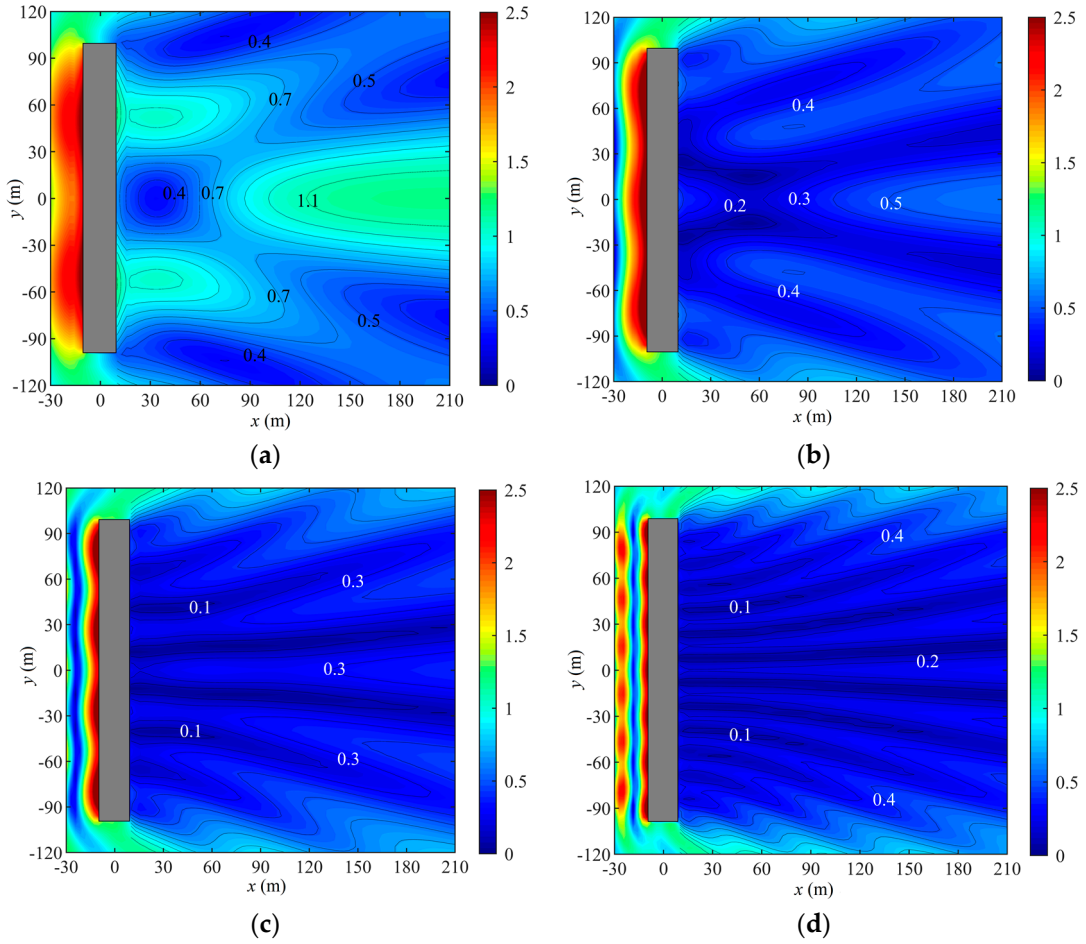

Figure 5. Contours of normalized wave elevation amplitude for FB#1 under regular waves, $\theta = 0°$, L/B = 10: (**a**) B/λ = 0.2, (**b**) B/λ = 0.27, (**c**) B/λ = 0.36, (**d**) B/λ = 0.63.

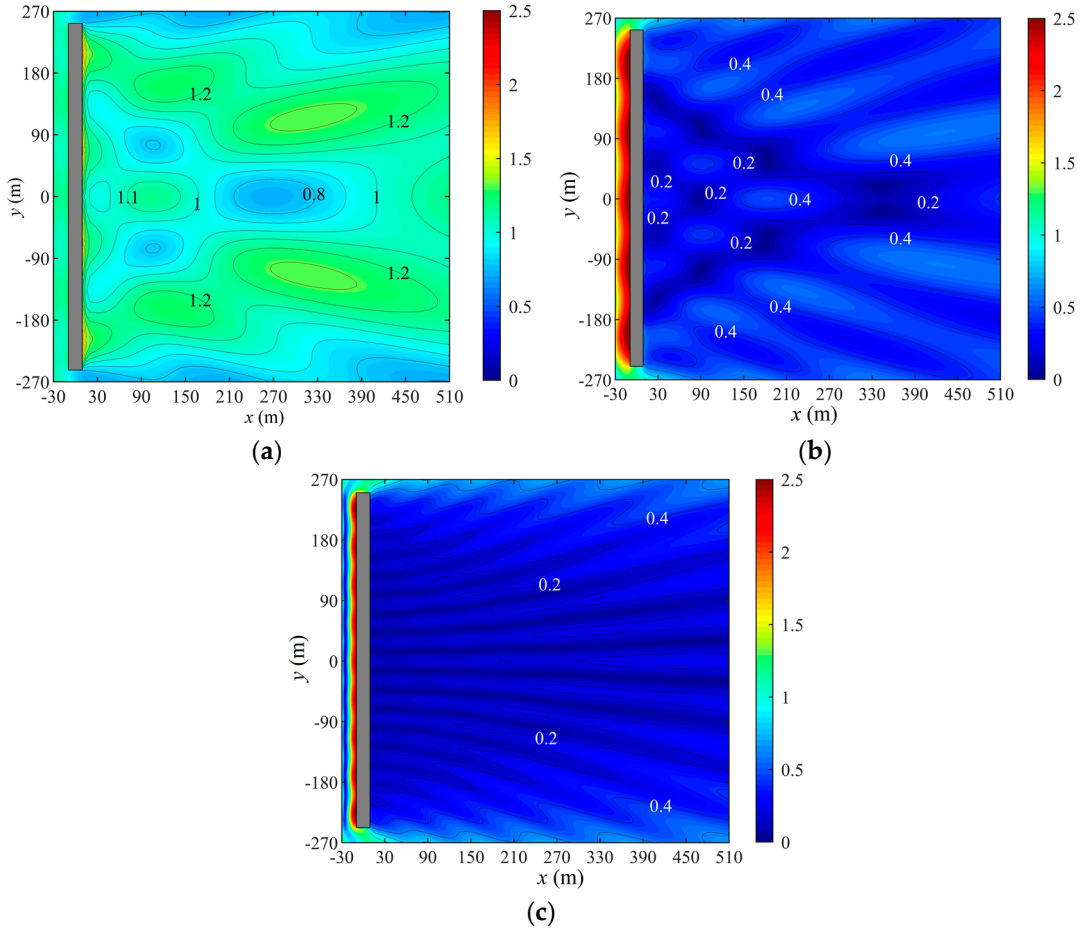

Figure 6. Contours of normalized wave elevation amplitude for FB#1L under regular waves, $\theta = 0°$, $L/B = 25$: (**a**) $B/\lambda = 0.15$, (**b**) $B/\lambda = 0.2$, (**c**) $B/\lambda = 0.36$.

Figure 5 also shows that the transmission coefficients vary significantly in the lee side of the breakwater. As this is not seen for the case of 2D floating breakwaters, the variation in the transmission coefficients should be due to the end effects (caused by the diffraction and radiation at the two ends of the finite length breakwater). The variation in the transmission coefficient is seen to decrease when λ decreases. This variation is also observed for the long floating breakwater FB#1L in Figure 6, but it is less significant. This means that the variation in the transmission coefficient decreases as L increases. In sum, it is observed that the variation in the transmission coefficient decreases as L/λ increases. Note that this variation was discussed for bottom-founded breakwaters [34]. When designing a 3D breakwater, minimizing the end effects should be desired for maximizing the wave attenuation performance of the breakwater. One possible way is to increase the length of the breakwater so that L/λ is large (e.g., $L/\lambda \approx 9$, as in Figure 6c). However, this solution is not always good because increasing the breakwater length translates to higher costs. Another possible way to minimize the end effects is to alter the plane shape of the 3D floating breakwater, e.g., arc-shaped breakwaters. This possibility is currently being investigated in our project and the results will be reported in the future.

Figure 5 also shows that the transmission coefficients within certain surface areas are larger than unity for relatively long waves (e.g., see Figure 5a). This was also observed from the experimental results for 3D breakwaters integrated with oscillating water column wave energy converters [11]. Such large transmission coefficients cannot be seen in the conventional 2D analysis of floating breakwaters (e.g., see results reported in [1,35]) due to the conservation of energy. This indicates that the large transmission coefficient phenomenon results from the 3D diffraction and radiation. Let us consider a 3D diffraction

problem where the motion of FB#1 is not considered. Figure 7 shows the transmission coefficients for the diffraction problem. It can be seen from Figure 7 that all the transmission coefficients in the wave field behind the breakwater have a smaller unity for FB#1 (without motion) and $B/\lambda = 0.2$. For this wave condition and the breakwater FB#1, the large transmission coefficient phenomenon occurs when the breakwater motion is considered (as seen in Figure 5a). For the considered B/λ ratio of 0.2, the corresponding wave frequency is close to the heave resonant frequency ($\omega \approx 0.75$ rad/s) of FB#1, as seen in Figure 8. The large transmission coefficient phenomenon also occurs for FB#1L and FB#2 when the wave frequency is close to the heave resonant frequency of the breakwater (about 0.65 rad/s for FB#1L and 0.75 rad/s for FB#2, as seen in Figure 8). The occurrence of such a phenomenon for FB#1L can be seen in Figure 6a for $B/\lambda = 0.15$ (or frequency of 0.65 rad/s). Figures 5 and 7 also show that due to the effect of 3D diffraction and radiation, the normalized wave elevation amplitude may be close to, or even higher than, 2 in the region just in front of the breakwater. This phenomenon was also observed in a previous numerical study [6] on 3D floating breakwaters.

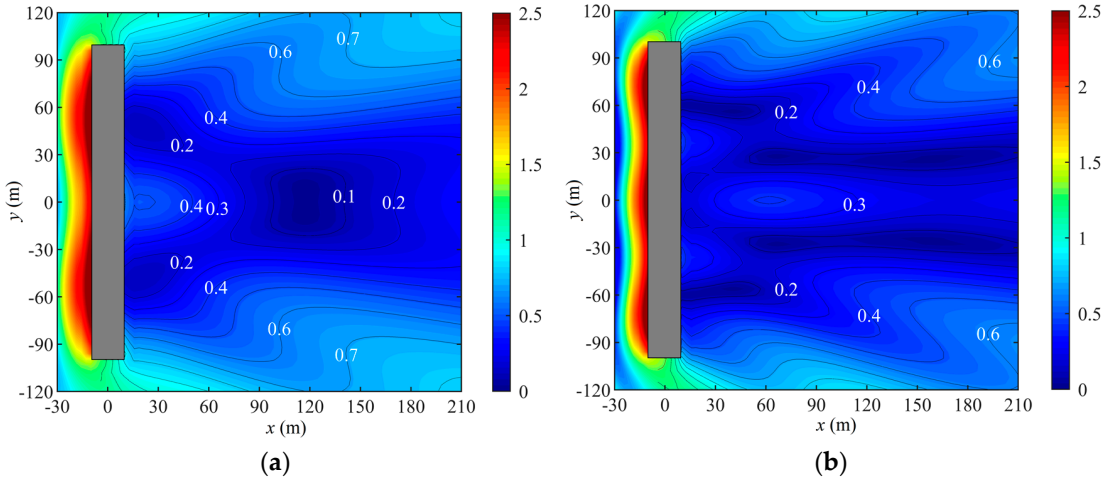

Figure 7. Contours of normalized wave elevation amplitude for FB#1 without motion (diffraction problem) under regular waves, $\theta = 0°$, $L/B = 10$: (**a**) $B/\lambda = 0.2$, (**b**) $B/\lambda = 0.27$.

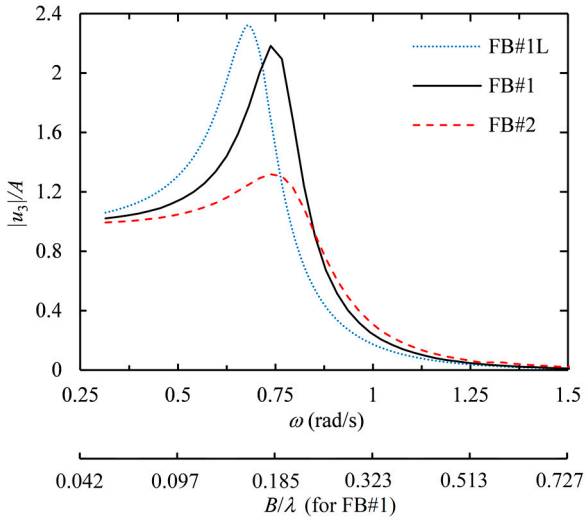

Figure 8. Normalized heave motion amplitude of FB#1, FB#2 and FB#1L for various wave frequencies.

Figures 9 and 10 present the contours of the normalized significant wave height for FB#1 and FB#1L. The normalized significant wave height is the ratio between the significant wave height of the disturbed waves (resulting from the interaction with the breakwaters)

and that of the incident wave. The contours of the normalized significant wave height behind the breakwaters reflect the transmission coefficients in irregular waves. It can be seen that the transmission coefficient for irregular waves also varies significantly in the lee side of the breakwaters.

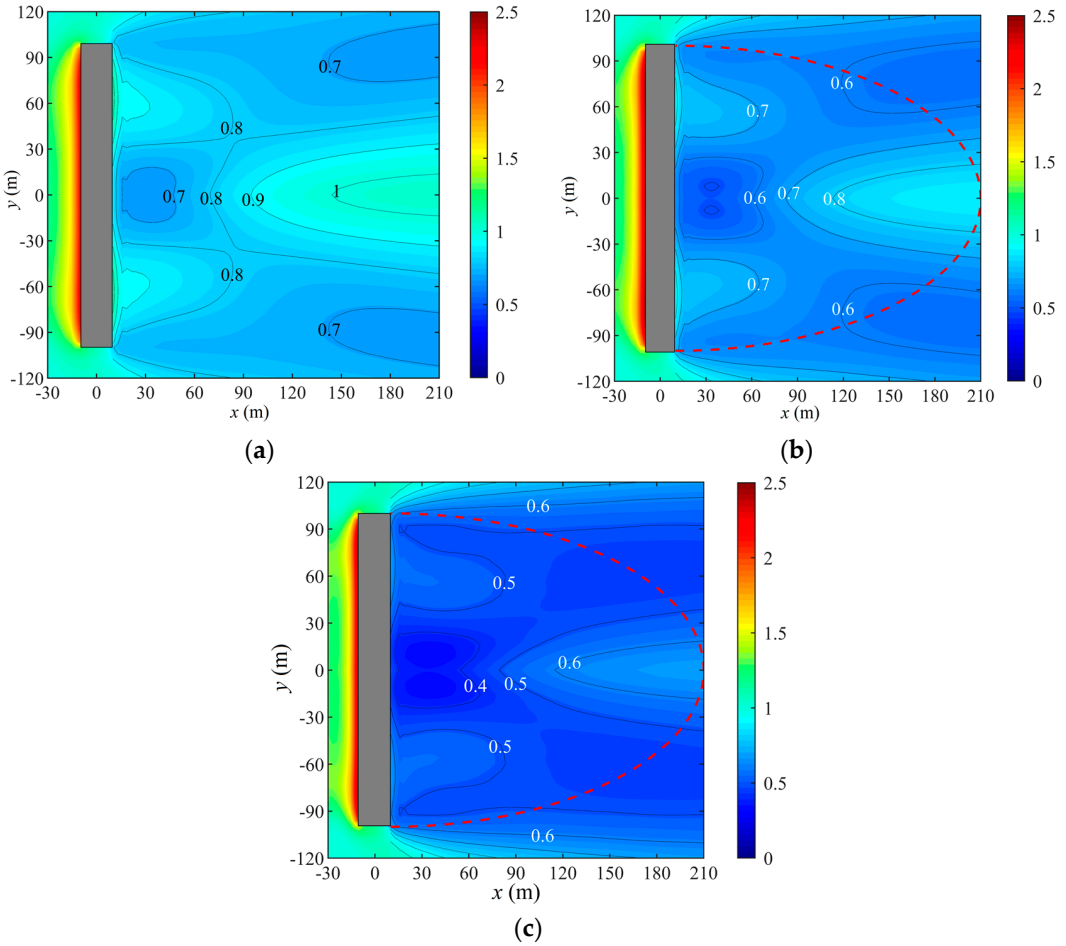

Figure 9. Contours of normalized significant wave height for FB#1 under irregular waves, $\theta = 0°$: (**a**) $\omega_s = 0.785$ rad/s, (**b**) $\omega_s = 0.911$ rad/s, (**c**) $\omega_s = 1.047$ rad/s. Semi-elliptical area bounded by lee side of breakwater and red dashed semi-ellipse is assumed to be the area of interest (in Section 3.2.2).

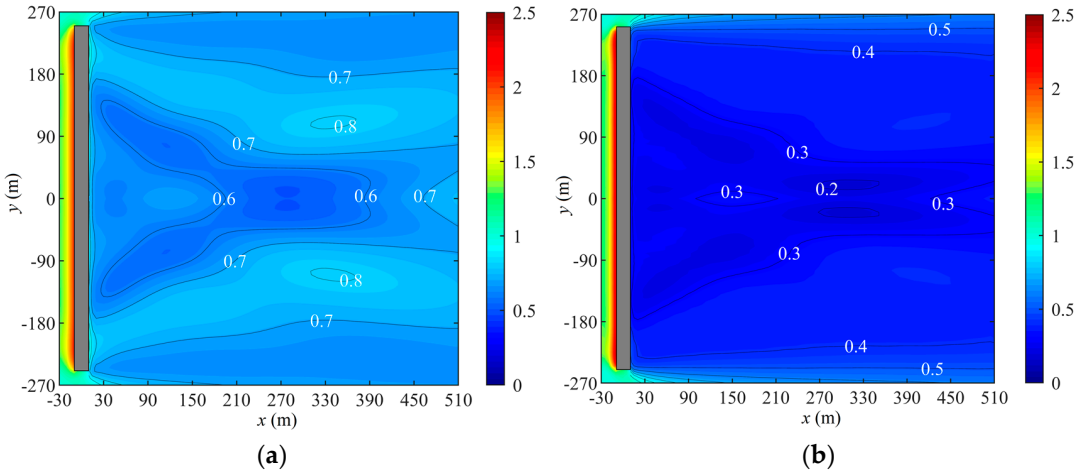

Figure 10. Contours of normalized significant height for FB#1L under irregular waves, $\theta = 0°$: (**a**) $\omega_s = 0.785$ rad/s, (**b**) $\omega_s = 1.047$ rad/s.

Figure 11 presents the difference ΔK_t between the transmission coefficient predicted for the representative regular wave and that for irregular waves. $\Delta K_t = K_{t,regular} — K_{t,irregular}$ where $K_{t,regular}$ and $K_{t,irregular}$ are, respectively, the transmission coefficients for representative regular waves and irregular waves. Figure 11 shows that the difference ΔK_t may be smaller than −0.4, and larger than 0.1. This finding for box-type heave-only breakwaters indicates that whilst the representative regular wave analysis is still adopted for predicting the wave attenuation performance in some design guidelines [4,17,19], the predicted performance may be significantly different from the actual performance of the breakwater in realistic irregular waves. More studies should be conducted in the future for different types of floating breakwaters and wave spectra to investigate their wave attenuation performance using the representative regular wave and irregular wave analyses.

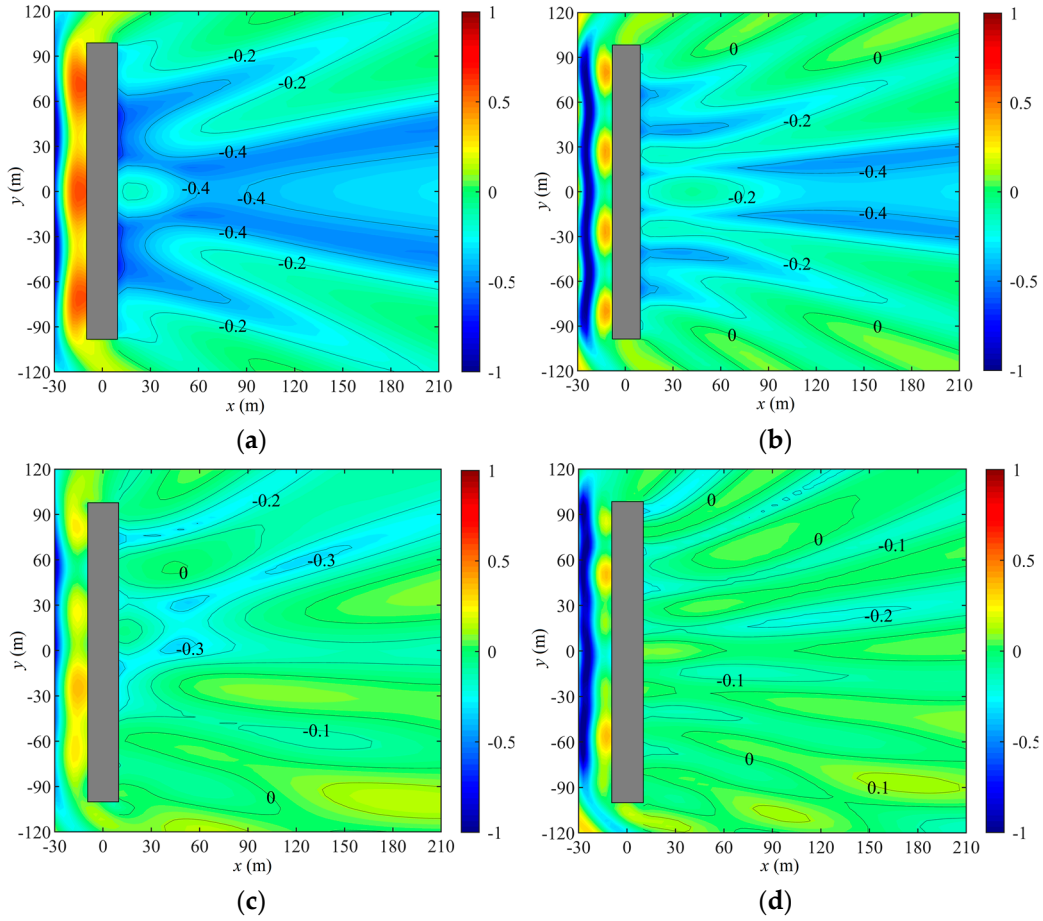

Figure 11. Difference (ΔK_t) in transmission coefficient of FB#1 under representative regular wave and irregular waves: (**a**) ω_s = 0.911 rad/s, θ = 0°, (**b**) ω_s = 1.047 rad/s, θ = 0°, (**c**) ω_s = 0.911 rad/s, θ = 30°, (**d**) ω_s = 1.047 rad/s, θ = 30°.

3.2. Evaluation of Wave Attenuation Performance

3.2.1. From Experimental Studies

In previous experimental studies, some researchers [7,9,11] evaluated the wave attenuation performance of 3D breakwaters by using the transmission coefficient taken at only one particular surface point for simplicity. However, the evaluation approach based on the transmission coefficient at only one surface point is generally not reasonable as it only gives a local result and does not reflect the global wave attenuation performance of a 3D breakwater. A better way is to evaluate the transmission coefficient over an area of interest. Thus, it is recommended to determine the transmission coefficients at multiple points within a surface area of interest. This approach was adopted by Loukogeorgaki et al. [8]. However, the required number of measured points and their locations have not been

clearly established. Another unanswered question is how to determine a representative transmission coefficient from transmission coefficients at multiple selected points. Perhaps, the maximum transmission coefficient (within the transmission coefficients at multiple measured points) may be taken as the representative value from safety consideration.

3.2.2. From Numerical Studies

In previous numerical studies, some researchers [10,13] used the mean transmission coefficient as the representative value for an area of interest. To examine this approach, consider the cases of Figure 9b,c. The surface area of interest is assumed to be a semi-elliptical area (as in Figure 9b,c). The area of interest is user-defined, and it may be of any shape and size. When pre-defining the area of interest, designers should consider their sheltered area of concern as well as the transmitted wave field. Here, a semi-elliptical area is adopted intuitively; we expect that the width of the sheltered area tends to be narrower far away from the lee side of a finite breakwater (due to the effect of the waves along the sides of the two ends of the breakwater).

Figure 12 presents the variations of the area percentage with respect to the transmission coefficient. Here, the area percentage corresponding to a considered transmission coefficient is defined as the percentage of the area of interest having the transmission coefficients smaller than the considered transmission coefficient. To obtain the results in Figure 12, we determined the transmission coefficients at about 8000 points evenly distributed within the area of interest. Each point was assumed to correspond to the same area. Figure 12 shows that only less than 60% of the area of interest has a transmission coefficient smaller than the mean transmission coefficient. If the mean transmission coefficient is considered as the representative one for the entire area of interest, the wave height determined from the incident wave height and the representative transmission coefficient is smaller than the actual wave heights for about 40% of the area of interest. Thus, the wave attenuation performance of the breakwater may be over-predicted. For greater safety, the area percentage should be higher, but not the highest (100%) to avoid the localization issue where the transmission coefficient at only one point is used for evaluating the wave attenuation performance. To obtain the representative transmission coefficient, the target area percentage needs to be specified. The area percentage is user-defined, and it is assumed to be 90% in this study. This area percentage (90%) can be acceptable when referring to the probability of wave heights smaller than the significant wave height (usually referred to as the representative wave height). Such a probability is about 86.5% by using the probability formula of the Rayleigh distribution [36]. By setting the target percentage area to 90%, the representative transmission coefficient $K_{t,90\%}$ for the case in Figure 12a is about 0.79, which is larger than the mean transmission coefficient by about 20% but smaller than the maximum transmission coefficient by about 10%. Note that the approach to determine the representative transmission coefficient based on the area percentage may also be applicable for experimental studies if the profile of wave elevations within the area of interest can be captured (such as by using stereo-videogrammetry [37]).

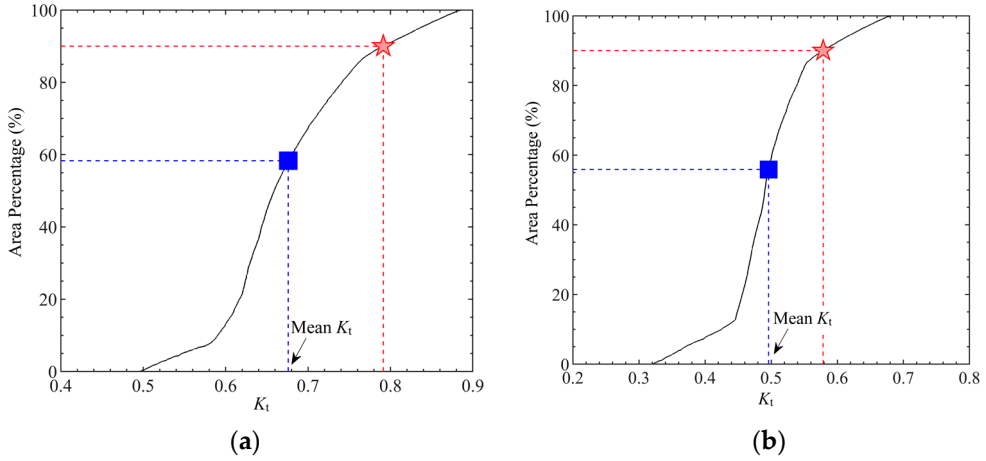

Figure 12. Transmission coefficient versus area percentage (black solid line) for FB#1, $\theta = 0°$, irregular wave: (**a**) $\omega_s = 0.911$ rad/s, (**b**) $\omega_s = 1.047$ rad/s. Square blue marker indicates mean transmission coefficient and corresponding area percentage. Red star marker indicates 90% area percentage and corresponding transmission coefficient.

Next, we investigate the representative transmission coefficients of FB#1, FB#1L and FB#2 in regular and irregular waves. The area of interest is assumed to be a semi-elliptical area where the ellipse's equation is $\frac{(x-B/2)^2}{L^2} + \frac{y^2}{(L/2)^2} = 1$ (e.g., see Figure 9b). Note that the area of interest for FB#1 is equal to that of FB#2, but smaller than that for FB#1L by a factor of 6.25. For reference, the breakwater FB#1L* is also considered. This breakwater is similar to FB#1L, but its considered area of interest is equal to that of FB#1. The target area percentage is set to 90%. Figure 13 shows the representative transmission coefficients $K_{t,90\%}$ for various wave frequencies. It can be seen that for regular waves, FB#1 is generally more effective than FB#2 in attenuating incident waves when $\omega > 0.78$ rad /s, but it is less effective for longer waves. This is expected as the width of the breakwater has to be larger for attenuating wave forces for longer waves. For $\omega > 0.78$ rad /s, the difference in the wave attenuation performance between the two breakwaters is up to about 39%. For irregular waves with $\omega_s > 0.78$ rad /s, the difference is much smaller (less than 10%).

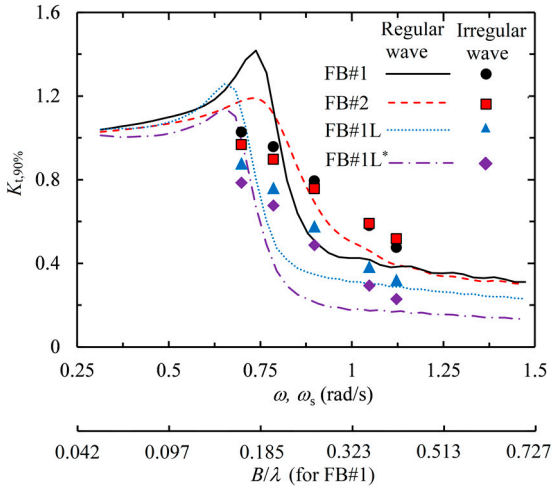

Figure 13. Representative transmission coefficients $K_{t,90\%}$ for FB#1, FB#1L and FB#2 in regular and irregular waves.

Figure 13 also shows that FB#1L is generally significantly more effective than FB#1 in attenuating incident waves (even though its area of interest is 6.25 times larger). The wave attenuation performance of the longer breakwater is even higher when the area of interest is

equal to that of FB#1 (see the transmission coefficients for FB#1L*). The significant difference in the wave attenuation performance between these two breakwaters of different lengths implies that it is necessary to perform a 3D hydrodynamic analysis of finite breakwaters so that the breakwater end effects on the wave attenuation performance is fully accounted for. The use of a 2D analysis for a floating breakwater with finite length may result in a non-conservative prediction (i.e., overprediction) of the wave attenuation performance.

Figure 14 shows the representative transmission coefficient $K_{t,90\%}$ for the heave-only and motionless breakwaters FB#1 and FB#2. It can be seen that when the breakwaters are fixed, FB#2, with a larger width, is more effective than FB#1 in attenuating incident waves. Their associated representative transmission coefficients increase as the wave frequency decreases and are generally significantly lower than the representative transmission coefficients for the heave-only FB#1 and FB#2. The difference in the representative transmission coefficient between the motionless breakwaters and the heave-only breakwaters indicates the necessity of considering breakwater motions in the hydrodynamic analysis. Figure 14 also shows that the representative transmission coefficients for the motionless breakwaters (i.e., diffraction problems) are always smaller than unity, and the large transmission coefficient phenomenon ($K_{t,90\%} > 1$) only occurs for the heave-only breakwaters (i.e., combined diffraction-radiation problems). Such a large transmission coefficient phenomenon may result from the interaction between the diffracted waves and the radiated waves for wave frequencies close to the heave resonant frequency of the breakwater (as discussed in Section 3.1).

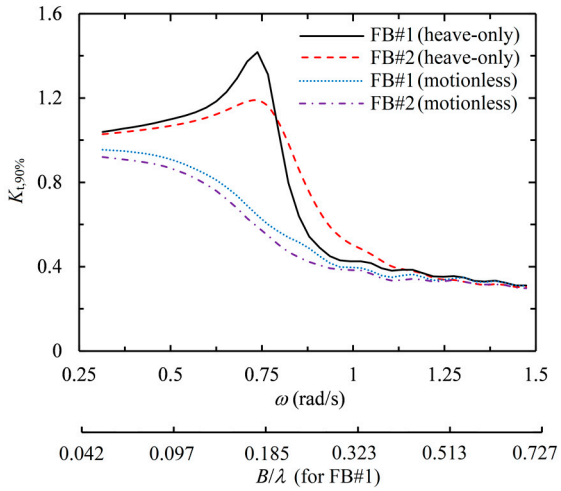

Figure 14. Representative transmission coefficients $K_{t,90\%}$ in regular waves for heave-only and motionless FB#1, FB#2.

Following the definition of significant wave height, we may alternatively define a representative transmission coefficient as the mean of the highest third of the transmission coefficients within the area of interest ($K_{t,1/3}$). Figure 15 shows the representative transmission coefficients $K_{t,1/3}$, $K_{t,85\%}$, $K_{t,90\%}$, $K_{t,95\%}$ for FB#1, FB#2, and FB#1L. Here, $K_{t,85\%}$, $K_{t,95\%}$ are the representative transmission coefficients corresponding to the area percentage of 85% and 95%, respectively. It can be seen that, for the cases considered, $K_{t,1/3}$ is close to $K_{t,90\%}$ and $K_{t,85\%}$, and it is smaller than $K_{t,95\%}$ by up to about 10% for irregular waves. Note that the largest transmission coefficient ($K_{t,100\%}$) is considered when determining $K_{t,1/3}$. This consideration is similar to the consideration of the largest wave height in the wave spectrum when determining the significant wave height. The consideration of the largest wave height is necessary as there is a possibility that the largest wave height occurs at any point within a prescribed surface area. However, for transmission coefficients, the largest transmission coefficient may occur at only certain areas such as near the lee side of the floating breakwater or the rear end of the area of interest, as seen in Figure 9b,c. This may make the consideration of the largest transmission coefficient less necessary

when compared to the consideration of the largest wave height. Thus, the definition of the representative transmission coefficient based on the area percentage (such as $K_{t,90\%}$) may be adopted, without considering the largest transmission coefficient as in the definition of $K_{t,1/3}$.

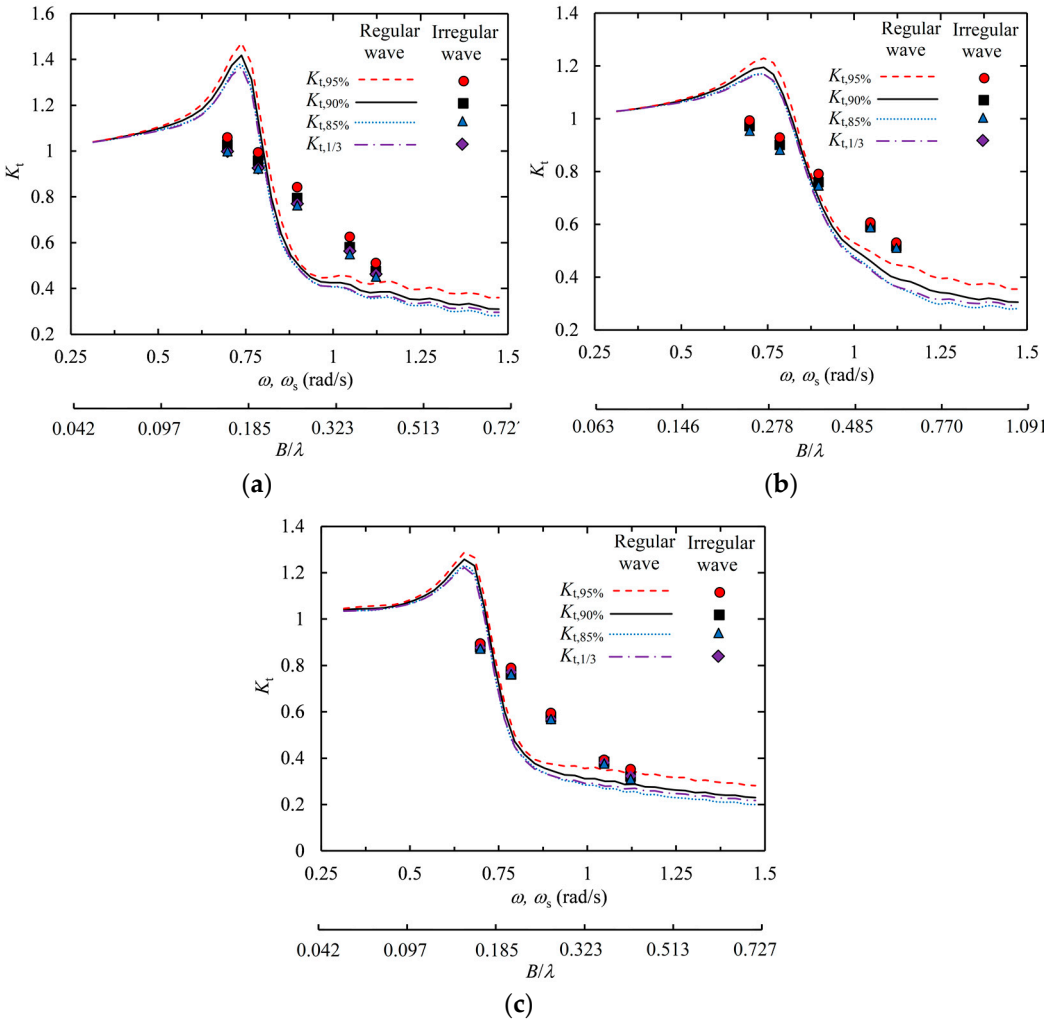

Figure 15. Representative transmission coefficients $K_{t,95\%}$, $K_{t,90\%}$, $K_{t,85\%}$, $K_{t,1/3}$ in regular and irregular waves: (**a**) FB#1, (**b**) FB#2, (**c**) FB#1L.

4. Conclusions

This paper numerically examines the transmitted wave field and possible approaches for quantifying the wave attenuation performance of 3D floating breakwaters in regular and irregular waves. Numerical hydrodynamic analyses were carried out for heave-only floating box-type breakwaters based on the classical linear hydrodynamic theory. It is found that using the transmission coefficient at a selected single surface point for evaluating the wave attenuation performance is unreasonable. In addition, it may be unsafe if the mean transmission coefficient within a prescribed area of interest is used for the evaluation of the wave attenuation performance. Instead, we propose a new index called the representative transmission coefficient for a prescribed area of interest. Within the area of interest, the probability of having transmission coefficients smaller than the representative transmission coefficient is set to a desired value, e.g., 90%. The proposed representative transmission coefficient allows one to easily compare the wave attenuation performances of different breakwater designs. Although the illustrative examples in this numerical study are only for straight box-type heave-only 3D floating breakwaters, the

representative transmission coefficient can be applied to evaluate the wave attenuation performance of any floating breakwaters.

Author Contributions: Conceptualization, all authors; methodology, H.P.N. and C.M.W.; validation, H.P.N. and C.M.W.; formal analysis, all authors; writing—original draft preparation, H.P.N., J.C.P., M.H. and C.M.W.; writing—review and editing, H.P.N., N.A., I.P. and D.H.; visualization, H.P.N.; funding acquisition, C.M.W. All authors have read and agreed to the published version of the manuscript.

Funding: This research was supported by the Australian Government through the Australian Research Council's Discovery Projects funding scheme (project DP170104546). The views expressed herein are those of the authors and are not necessarily those of the Australian Government or Australian Research Council.

Institutional Review Board Statement: Not applicable.

Informed Consent Statement: Not applicable.

Data Availability Statement: The data presented in this study are available from the corresponding author on reasonable request.

Conflicts of Interest: The authors declare no conflict of interest.

References

1. Dai, J.; Wang, C.M.; Utsunomiya, T.; Duan, W. Review of recent research and developments on floating breakwaters. *Ocean Eng.* **2018**, *158*, 132–151. [CrossRef]
2. He, F.; Zhang, H.; Zhao, J.; Zheng, S.; Iglesias, G. Hydrodynamic performance of a pile-supported OWC breakwater: An analytical study. *Appl. Ocean Res.* **2019**, *88*, 326–340. [CrossRef]
3. van der Meer, J.W.; Briganti, R.; Zanuttigh, B.; Wang, B. Wave transmission and reflection at low-crested structures: Design formulae, oblique wave attack and spectral change. *Coast. Eng.* **2005**, *52*, 915–929. [CrossRef]
4. Goda, Y. *Random Seas and Design of Maritime Structures*, 3rd ed.; World Scientific: Singapore, 2010.
5. Buccino, M.; del Vita, I.; Calabrese, M. Engineering Modeling of Wave Transmission of Reef Balls. *J. Waterw. Port Coastal Ocean Eng.* **2014**, *140*, 04014010. [CrossRef]
6. Diamantoulaki, I.; Angelides, D.C.; Manolis, G.D. Performance of pile-restrained flexible floating breakwaters. *Appl. Ocean Res.* **2008**, *30*, 243–255. [CrossRef]
7. Ji, C.Y.; Guo, Y.C.; Cui, J.; Yuan, Z.M.; Ma, X.J. 3D experimental study on a cylindrical floating breakwater system. *Ocean Eng.* **2016**, *125*, 38–50. [CrossRef]
8. Loukogeorgaki, E.; Yagci, O.; Kabdasli, M.S. 3D Experimental investigation of the structural response and the effectiveness of a moored floating breakwater with flexibly connected modules. *Coast. Eng.* **2014**, *91*, 164–180. [CrossRef]
9. Martinelli, L.; Ruol, P.; Zanuttigh, B. Wave basin experiments on floating breakwaters with different layouts. *Appl. Ocean Res.* **2008**, *30*, 199–207. [CrossRef]
10. Michailides, C.; Angelides, D.C. Modeling of energy extraction and behavior of a Flexible Floating Breakwater. *Appl. Ocean Res.* **2012**, *35*, 77–94. [CrossRef]
11. Howe, D.; Nader, J.R.; Macfarlane, G. Experimental investigation of multiple oscillating water column wave energy converters integrated in a floating breakwater: Wave attenuation and motion characteristics. *Appl. Ocean Res.* **2020**, *99*, 102160. [CrossRef]
12. Kashiwagi, M.; Mahmuddin, F. Numerical analysis of a 3D floating breakwater performance. In Proceedings of the 22nd (2012) International Offshore and Polar Engineering Conference, Rhodes, Greece, 17–23 June 2012.
13. Wang, C.M.; Han, M.M.; Lyu, J.; Duan, W.H.; Jung, K.H.; An, S.K. Floating Forest: A Novel Concept of Floating Breakwater-Windbreak Structure. *Lect. Notes Civ. Eng.* **2020**, *41*, 219–234.
14. Bretschneider, C.L. *Wave Variability and Wave Spectra for Wind-Generated Gravity Waves*; US Army Corps of Engineers: Washington, DC, USA, 1959.
15. Prendergast, J.; Li, M.; Sheng, W. A study on the effects of wave spectra on wave energy conversions. *IEEE J. Ocean. Eng.* **2020**, *45*, 271–283. [CrossRef]
16. Saulnier, J.-B.; Ricci, P.; Pontes, M.T.; Falcão, A.F.D.O. Spectral Bandwidth and WEC Performance Assessment. In Proceedings of the 7th European Wave and Tidal Energy Conference, Porto, Portugal, 2007.
17. Ruol, P.; Martinelli, L.; Pezzutto, P. Formula to Predict Transmission for π-Type Floating Breakwaters. *J. Waterw. Port. Coastal. Ocean Eng.* **2013**, *139*, 1–8. [CrossRef]
18. Overseas Coastal Area Development Institute of Japan, Technical Standards and Commentaries for Port and Harbour Facilities in Japan, 2009. Available online: https://ocdi.or.jp/tec_st/tec_pdf/tech_00H.pdf (accessed on 15 February 2021).
19. US Army Corps of Engineers (US ACE), Shore Protection Manual, 1984. Available online: https://usace.contentdm.oclc.org/digital/collection/p16021coll11/id/1934/ (accessed on 15 February 2021).

20. Tay, Z.Y. Performance and wave impact of an integrated multi-raft wave energy converter with floating breakwater for tropical climate. *Ocean Eng.* **2020**, *218*, 108136. [CrossRef]
21. Permanent International Association of Navigation Congresses (PIANC), Floating Breakwaters: A Practical Guide for Design and Construction, 1994. Available online: https://www.pianc.org/publications/marcom/floating-breakwaters-a-practical-guide-for-design-and-construction (accessed on 10 January 2021).
22. Sannasiraj, S.A.; Sundar, V.; Sundaravadivelu, R. Mooring forces and motion responses of pontoon-type floating breakwaters. *Ocean Eng.* **1998**, *25*, 27–48. [CrossRef]
23. Zhang, H.; Zhou, B.; Vogel, C.; Willden, R.; Zang, J.; Zhang, L. Hydrodynamic performance of a floating breakwater as an oscillating-buoy type wave energy converter. *Appl. Energy* **2020**, *257*, 113996. [CrossRef]
24. Kim, K.-T.; Lee, P.-S.; Park, K.C. A direct coupling method for 3D hydroelastic analysis of floating structures. *Int. J. Numer. Methods Eng.* **2013**, *96*, 842–866. [CrossRef]
25. Nguyen, H.P.; Dai, J.; Wang, C.M.; Ang, K.K.; Luong, V.H. Reducing hydroelastic responses of pontoon-type VLFS using vertical elastic mooring lines. *Mar. Struct.* **2018**, *59*, 251–270. [CrossRef]
26. Liu, G.R.; Quek, S. *The Finite Element Method: A Practical Course*; Butterworth Heinemann: Oxford, UK, 2003.
27. Sarpkaya, T.; Isaacson, M. *Mechanics of Wave Forces on Offshore Structures*; Van Nostrand Reinhold Co.: New York, NY, USA, 1981.
28. Faltinsen, O.M. *Sea Loads on Ships and Offshore Structures*; Cambridge University Press: Cambridge, UK; New York, NY, USA, 1990.
29. Nguyen, H.P.; Wang, C.M. Oscillating Wave Surge Converter-Type Attachment for Extracting Wave Energy While Reducing Hydroelastic Responses of Very Large Floating Structures. *J. Offshore Mech. Arct. Eng.* **2020**, *142*, 042001. [CrossRef]
30. Nguyen, H.P.; Wang, C.M. Heaving wave energy converter-type attachments to a pontoon-type very large floating structure. *Eng. Struct.* **2020**, *219*, 110964. [CrossRef]
31. Ustunomiya, T. Hydroelastic analysis of VLFS. In *Very Large Floating Structures*; Wang, C.M., Watanabe, E., Utsunomiya, T., Eds.; Taylor and Francis: New York, NY, USA, 2008.
32. Macagno, E. Houle dans un canal présentant un passage en charge. *La Houille Blanche* **1953**, *1*, 10–37. [CrossRef]
33. Koutandos, E.; Prinos, P.; Gironella, X. Floating breakwaters under regular and irregular wave forcing: Reflection and transmission characteristics. *J. Hydraul. Res.* **2005**, *43*, 174–188. [CrossRef]
34. Penney, W.G.; Price, A.T. Part I. The diffraction theory of sea waves and the shelter afforded by breakwaters. *Philos. Trans. R. Soc. London Ser. A Math. Phys. Sci.* **1952**, *244*, 236–253.
35. Zhao, X.L.; Ning, D.Z.; Zou, Q.P.; Qiao, D.S.; Cai, S.Q. Hybrid floating breakwater-WEC system: A review. *Ocean Eng.* **2019**, *186*, 106126. [CrossRef]
36. Yamashita, S. Wave phenomenon and properties. In *Very Large Floating Structures*; Wang, C.M., Watanabe, E., Utsunomiya, T., Eds.; Taylor and Francis: New York, NY, USA, 2008.
37. Winship, B. Investigation on the Use of Wall Reflections to Simulate Wave Energy Converter Array Effects. Ph.D. Thesis, University of Tasmania, Hobart, Australia, 2019.